Reactions of copper(II) bromide with 2,6-diacetylpyridine bis(phenylhydrazone) (L) – Molecular and crystal structures of L and its mixed-valence complex [Cu^{II}L$_2$][Cu^{I}$_2$Br$_4$]

MARKO V. RODIĆ[1*#], MIRJANA M. RADANOVIĆ[1#], DRAGANA V. GAZDIĆ[1],
VUKADIN M. LEOVAC[1#], BERTA BARTA HOLLÓ[1#], VIDAK RAIČEVIĆ[1#],
SVETLANA K. BELOŠEVIĆ[2#], BILJANA KRÜGER[3]
and LJILJANA S. VOJINOVIĆ-JEŠIĆ[1#]

[1]University of Novi Sad, Faculty of Sciences, Trg Dositeja Obradovića 3, 21000 Novi Sad, Serbia, [2]Faculty of Technical Sciences, University of Priština, Knjaza Miloša 7, 38220 Kosovska Mitrovica, Serbia and [3]University of Innsbruck, Institute of Mineralogy and Petrography, Innrain 52, 6020 Innsbruck, Austria

Abstract: Utilizing X-ray crystallography, the crystal and molecular structures of 2,6-diacetylpyridine bis(phenylhydrazone) (**L**) were determined. The energetics of the intermolecular interactions in the crystal structure were assessed with computational methods, revealing that dispersion interactions are dominant. The basic structural unit of the crystal packing was revealed to be the herring-bone type arrangement of **L** molecules. Assignation of the IR spectrum of **L** with the aid of DFT calculations was performed. Furthermore, new reactions of **L** with CuBr$_2$ in different solvents are described, which led to the synthesis of the mixed Cu(II)–Cu(I) complex with the formula [Cu^{II}L$_2$][Cu^{I}$_2$Br$_4$] (**1**), and its structural characterization. In the complex cation, two molecules of tridentate N$_3$ ligand are meridionally arranged in a very distorted octahedral environment of a Cu(II) ion. In [Cu$_2$Br$_4$]$^{2-}$, the bromide ions are arranged in a trigonal-planar geometry around each copper(I) atom. Finally, for ligand, **1**, and the previously synthesized complex [Cu**L**$_2$]Br$_2$, the thermal properties were examined. The thermal stability of the complexes were lower than that of the ligand and decrease in the order: **L** (250 °C) > [Cu**L**$_2$]Br$_2$ (221 °C) > [Cu^{II}L$_2$][Cu^{I}$_2$Br$_4$] (212 °C). The differences in thermal stability of the complexes are due to differences in the packing efficacy of the constitutional ions.

Keywords: copper(I); Schiff bases; tridentate coordination mode; X-ray crystallography; DFT.

INTRODUCTION

Hydrazones represent a large group of organic compounds formed by the condensation of carbonyl compounds with hydrazine or its derivatives. Considering the variety of both carbonyl compounds and hydrazine derivatives, the large number of reported hydrazones is not surprising. These compounds are interesting for research not only from the theoretical point of view but also due to the possibility of their application in different areas (wide range of biological activity, analytical reagents, catalysis, *etc.*). This resulted in the publication of numerous scientific papers, reviews, and monographs concerning this group of compounds.[1–9]

Having different donor atoms (N, O, S, P, *etc.*) to coordinate the metal ions rendered this group of compounds a very interesting topic for coordination chemists.[2,10] For coordination chemists, a significant ligand precursor is 2,6-diacetylpyridine, which, depending on the hydrazine derivative it is condensed with, can yield bis(hydrazones) of differing denticity. The most numerous are those that act as tridentate and pentadentate ligands.[11–14]

Some time ago, synthesis, spectroscopic and magnetic characterization of mono- and bis(ligand) complexes of Fe(II), Co(II), Ni(II) and Cu(II) with the tridentate N_3 ligand, 2,6-diacetylpyridine bis(phenylhydrazone) of general formulae $[M(\mathbf{L})Cl_2]$ and $[M\mathbf{L}_2](ClO_4)_2$ were described.[11] Recently, complexes with the title ligand, *i.e.*, $[Co\mathbf{L}_2]I_2$[15] and $[Cu\mathbf{L}_2]Br_2$,[16] have been synthesized and structurally characterized, which represent the only metal complexes with this ligand to be characterized by SC-XRD so far. As a continuation of research on the coordinating properties of 2,6-diacetylpyridine bis(phenylhydrazone), in this paper, its new reactions with $CuBr_2$ in different solvents are described, which led to the synthesis, structure, and characterization of a mixed Cu(II)–Cu(I) complex with the formula $[Cu^{II}\mathbf{L}_2][Cu^I_2Br_4]$. Thermal properties were also examined, both for the ligand and the complex $[Cu\mathbf{L}_2]Br_2$ synthesized earlier.

EXPERIMENTAL

Reagents

All chemicals used were commercially available products of analytical reagent grade and were used without further purification. The ligand, 2,6-diacetylpyridine bis(phenylhydrazone), **L**, was synthesized according to a previously described procedure.[15]

*Preparation of single-crystals of 2,6-diacetylpyridine-bis(phenylhydrazone) (**L**)*

Single crystals suitable for X-ray crystallographic analysis were obtained by diffusion of Et_2O to a concentrated acetonic solution of the ligand.

*Synthesis of the complex $[Cu^{II}\mathbf{L}_2][Cu^I_2Br_4]$ (**1**)*

To 20 cm^3 of Me_2CO, 44 mg (0.2 mmol) of $CuBr_2$ was added and slightly heated. To this greenish suspension, 34 mg (0.1 mmol) of **L** was added and the heating was continued for 5 min, during which the solution obtained a red color. The resulting solution was left at room temperature and after three days, red needle-like microcrystals of undefined composition and

black prismatic single crystals of complex **1** were filtered off and washed with Me_2CO. Yield of the mixture: 50 mg.

*Synthesis of the complex [Cu^{II}**L**$_2$][Cu$^I_2$Br$_4$] (1) (from MeOH solution)*

A mixture of 34 mg (0.1 mmol) of **L** and 44 mg (0.2 mmol) of $CuBr_2$ was dissolved in 10 cm^3 of warm MeOH and evaporated to a small volume. The obtained black ribbed-plate-like crystals were filtered off and washed with MeOH. Yield: 30 mg (50 %).

Analytical methods

Elemental analyses (C, H and N) of air-dried compounds were performed by standard micro-methods. Molar conductivity measurements of a freshly prepared DMF solution of the complex (c = 1 mmol dm^{-3}) were performed on a Jenway 4010 conductivity meter. IR spectra were recorded on a Nicolet iS20 (Thermo Scientific) FTIR spectrophotometer, in the range of 400–4000 cm^{-1}, using the KBr pellet technique. ^{1}H- and ^{13}C$\{^1$H$\}$-NMR spectra were acquired on a Bruker Avance III spectrometer equipped with a CryoProbe Prodigy probe-head, operating at 400 and 100.6 MHz, respectively. The spectra were assigned using 2D techniques (gradient ^{1}H–^{1}H COSY, HSQC and HMBC), which were recored using the built-in Bruker pulse sequences. Coupling constants were determined using spin simulation. Thermal data were collected using a TA Instruments SDT Q600 thermal analyzer coupled to a Hiden Analytical HPR20/QIC mass spectrometer. The decomposition was followed from room temperature to 700 °C at a heating rate of 20 °C min^{-1} under a nitrogen carrier gas (flow rate = 100 cm^3 min^{-1}). Sample holder/reference: alumina crucible/empty alumina crucible. Sample mass 2.5–3 mg. TG–MS measurements were performed from room temperature to 350 °C at a heating rate of 10 °C min^{-1} under an argon carrier gas (flow rate = 50 cm^3 min^{-1}). Selected ions for *m/z* 1–58 were monitored in the multiple ion detection mode (MID).

Analytical and spectral data of the synthesized compounds are given in Supplementary material to this paper.

Crystal structure determination

Diffraction experiments were performed on a dual source (MoKα and CuKα X-radiation) Gemini R Ultra diffractometer, equipped with a Ruby CCD detector (Oxford Diffraction). Single crystals were cooled to 170 K by a flux of dry air. The CrysAlisPro was used for the experiment setup and data reduction.[17] Crystal structures were solved with SHELXT[18] and refined by using SHELXL-2018[19] interfaced with ShelXle.[20] Pertinent crystallographic and refinement details are listed in Table S-I of the Supplementary material. The crystallographic data are deposited at the Cambridge Crystallographic Data Centre. CCDC Nos.: 2123008 for **L** and 2123007 for **1**. These data are available free of charge *via* https://www.ccdc.cam.ac.uk/structures/.

Hirshfeld surface analysis and intermolecular interaction energies estimate

Hirshfeld surface calculations were performed with Crystal Explorer 2020.[21] Intermolecular interaction energies were calculated, and parsed to electrostatic, dispersion, polarization, and repulsion terms, using CE-B3LYP model energies[22] with Crystal Explorer 2020,[21] and utilizing TONTO[23] as a backend. Calculations were performed for intermolecular dimers comprised of a selected molecule and all its nearest neighbors defined by the Hirshfeld surface.

Computational methods

All density functional calculations (DFT) calculations were performed with GAMESS US.[24] Equilibrium geometry of an isolated 2,6-diacetylpyridine bis(phenylhydrazone) molecule was optimized using B3LYP exchange-correlation functional, and 6-31G(d,p) basis set.
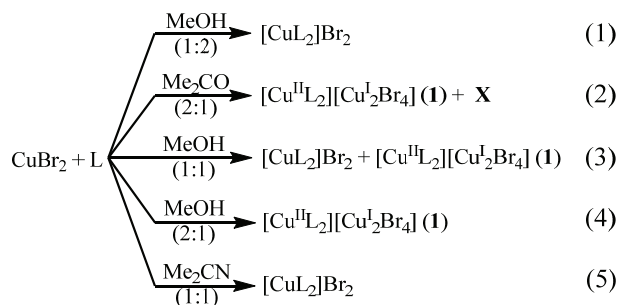
The initial structure was chosen to represent the molecular conformation found in the crystal structure. The ground state was confirmed by the fact that vibrational analysis resulted only in positive frequencies. Partial assignment of IR bands was performed by visual inspection of molecular vibrations with MacMolPlt.[25]

RESULTS AND DISCUSSION

Syntheses and characterization

A previously described synthesis of the ligand was performed,[15] *i.e.*, warm EtOH solutions of stoichiometric amounts of 2,6-diacetylpyridine and phenyl-hydrazine hydrochloride were reacted in the presence of an excess of LiOAc. This resulted in the formation of microcrystals of the ligand. Crystals suitable for X-ray diffraction were prepared by slow vapor diffusion of Et_2O into a concentrated acetonic solution of the ligand.

In a previous paper,[15] the synthesis of the Cu(II) complex with 2,6-diacetyl-pyridine bis(phenylhydrazone) of the formula $[CuL_2]Br_2$ was reported. This complex was obtained in the reaction of MeOH solutions of $CuBr_2$ and **L** in a 1:2 mole ratio (Scheme 1). Herein, the observation that the composition of the obtained complexes depends not only on the mole ratio of the reactants but also on the nature of the solvent is reported, which is corroborated by results achieved by examining different reaction conditions (Scheme 1).

$$CuBr_2 + L \begin{cases} \xrightarrow[\text{(1:2)}]{\text{MeOH}} [CuL_2]Br_2 \quad (1) \\ \\ \xrightarrow[\text{(2:1)}]{\text{Me}_2\text{CO}} [Cu^{II}L_2][Cu^I_2Br_4]\ (\mathbf{1}) + \mathbf{X} \quad (2) \\ \\ \xrightarrow[\text{(1:1)}]{\text{MeOH}} [CuL_2]Br_2 + [Cu^{II}L_2][Cu^I_2Br_4]\ (\mathbf{1}) \quad (3) \\ \\ \xrightarrow[\text{(2:1)}]{\text{MeOH}} [Cu^{II}L_2][Cu^I_2Br_4]\ (\mathbf{1}) \quad (4) \\ \\ \xrightarrow[\text{(1:1)}]{\text{Me}_2\text{CN}} [CuL_2]Br_2 \quad (5) \end{cases}$$

Scheme 1. Reactions of $CuBr_2$ and **L**.

The reaction of $CuBr_2$ and **L** in a 2:1 mole ratio in warm Me_2CO gave a mixture of black prismatic single crystals of the formula $[Cu^{II}L_2][Cu^I_2Br_4]$ (**1**) and thin red needle-like crystals of undefined composition (**X**). Crystals of **1** were suitable for SC-XRD, by which the structure of the obtained complex was unambiguously proven (*vide infra*). Based on elemental analysis and IR spectra, it was not possible to unequivocally propose a molecular formula for **X**.

When the reaction was performed in MeOH in a 2:1 mole ratio, only black ribbed-plate-like crystals of **1** were formed. The quality of these was not sufficiently high for SC-XRD, but based on the results of elemental analysis and

identity of its IR spectrum with the spectrum of **1**, the same composition and coordination formula was proposed.

A mixture of the crystals of **1** and previously characterized $[CuL_2]Br_2$ was formed in the reaction of a MeOH solution of the reactants present in a 1:1 mole ratio. Finally, if acetonitrile was used as the solvent instead of MeOH in mole ratio 1:1, only the bis(ligand) complex $[CuL_2]Br_2$ formed.

Complex **1** is stable at higher temperatures (decomp. 212 °C) and shows appreciable solubility in DMF, while it is only partially soluble in alcohols and acetone, and virtually insoluble in H_2O. The molar conductivity of a DMF solution of the complex had a value of 134 S cm^2 mol^{-1} and corresponds to 2:1 type of electrolytes,[26] which could be explained by the partial decomposition of the complex anion.

In the IR spectrum of the ligand, as well as the spectrum of the complex in the high-energy region (>3000 cm^{-1}), there was only one band that could undoubtedly be ascribed to ν(NH) vibrations; it is located at 3342 cm^{-1} in the spectrum of the ligand and at 3271 cm^{-1} in the spectrum of the complex.

The presence of an IR band corresponding to C=N(imine) stretching is often taken as an indication of whether coordination of the imine nitrogen had occured.[27] Therefore, it is of importance to assign this vibration to an appropriate band(s) in the IR spectrum of **L**. In this study, this step was performed using the results of DFT calculations, along with the assignment of some other characteristic IR bands. The optimized geometry of **L** closely matches the experimentally determined one, as mean absolute deviations of non-hydrogen involved bond lengths and valence angles are 0.011 Å and 0.61°, respectively. Therefore, the calculated vibrational frequencies derived from a theoretical molecular structure may be regarded as reliable.

The very strong band at 1602 cm^{-1} corresponds to C–C stretching modes of phenyl rings. The stretching of the C=N fragment is coupled both to phenyl rings valence vibrations and pyridine ring valence vibrations, and appears as a shoulder in the IR spectrum at 1592 cm^{-1} and a strong band at 1563 cm^{-1}, respectively. The strong sharp band at 1508 cm^{-1} corresponds to in-plane N–H deformations, and the presence of this band may be used to assign the ionic state of **L** in complexes. A medium-intensity band at 1491 cm^{-1} corresponds to phenyl rings C–H in-plane deformations. Stretching vibration of the hydrazine N–N fragment corresponds to a very strong band at 1165 cm^{-1}. Two strong bands, inherent of monosubstituted benzene rings (*i.e.*, phenyl group), associated with ν(C–H) vibrations, can be found at 748 and 694 cm^{-1}.[28] Finally, in-plane pyridine ring deformation, which is metal--sensitive and can reveal coordination of the pyridine nitrogen if shifted to higher wavenumbers,[29] corresponds to the band at 647 cm^{-1}. Other bands in the IR spectrum of the ligand are of little importance for studies of its coordination chemistry and are not discussed.

In the IR spectrum of **1**, the mentioned shoulder at 1592 cm^{-1} is nonexistent, but more importantly, the band at 1563 cm^{-1} is shifted to lower wavenumbers (1518 cm^{-1}), which is in agreement with the observation that coordination of both the imine nitrogen atom and pyridine nitrogen atom lowers the strengths of these bonds.

Crystal structure of 2,6-diacetylpyridine bis(phenylhydrazone) (L)

The molecular structure of **L** is depicted in Fig. 1. 2,6-Diacetylpyridine bis-(phenylhydrazone) displays roughly planar conformation in the crystal structure, with an s-*trans* arrangement of substituents around C1–C6, C5–C8, as well as N1–N3 and N4–N5 bonds (an all-*trans* conformation). The structures in the Cambridge Structural Database (CSD)[30] KEWWOB[31] and URINOZ[32] correspond to compounds [HL]NO$_3$ and [HL]ClO$_4$ containing protonated **L**, in which both hydrazone moieties are in a conformation in which the arrangement around equivalent C–C bonds is s-*cis*, implying that conformations of **L** in its neutral and protonated forms are significantly different.
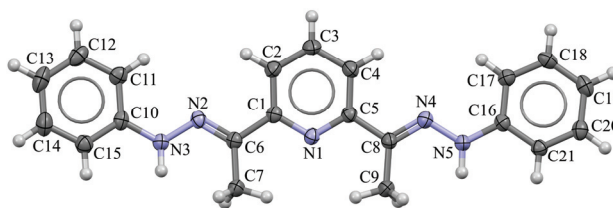

Fig. 1. Molecular structure of **L** with the atom numbering scheme.

Mogul validation of all structural parameters of **L** (bond lengths, valence, and torsions angles as well as ring conformations) against CSD structures having similar fragments indicated that they are completely within the expected range.

The analysis of atom–atom specific contacts by Hirshfeld surface decomposition reveals that major intermolecular contacts are of the type H⋯H (50.8 %), C⋯H (21.2 %) and N⋯H (14.6 %). Enrichment ratios[33] represent an elegant way to judge the propensity of pairs of chemical species to form crystal-packing interactions. Their values for the crystal structure of **L** are listed in Table S-II of the Supplementary material. It can be seen that C⋯C, N⋯N and C⋯N contacts are strongly avoided, while H⋯H contacts are slightly depressed in the crystal structure (E_{HH} = 0.90), even though H⋯H contacts comprise the majority of the Hirshfeld surface of the molecule. On the contrary, enrichment ratios for C⋯H and N⋯H contacts are significantly higher than unity (E_{CH} = 1.31, E_{NH} = 1.31), indicating that these interatomic contacts are favored in the crystal structure. It is interesting to note that, even though **L** has two potential hydrogen-bond donors (hydrazine nitrogen atoms), and three potential acceptors (pyridine and imine nitrogen atoms), these hydrogen bonds are not realized in the crystal structure.

It is the lack of common atom–atom intermolecular contacts, and related intermolecular features, such as CH···π or stacking interactions, that causes difficulties in recognizing the structural determinants of the crystal packing. To overcome this hurdle, the assessment of pairwise intermolecular energies was performed by CE-B3LYP model energies, and the results are summarized in Table I and Fig. S-1 of the Supplementary material.

TABLE I. Summary of intermolecular interaction energies (kJ mol^{-1}) of the unique molecular pairs constituting the first coordination sphere for **L** calculated using CE-B3LYP model energy; N, the number of interactions equals 2; R is the distance between molecular centroids. The relevant space group symmetry operation is reported without translation. Total interaction energy is calculated by addition of scaled individual components: $E_{tot} = k_{ele}E_{ele} + k_{pol}E_{pol} + k_{dis}E_{dis} + k_{rep}E_{rep}$, where $k_{ele} = 1.057$, $k_{pol} = 0.740$, $k_{dis} = 0.871$, and $k_{rep} = 0.618$[22]

Symmetry operation	R / Å	Energy				
		E_{ele}	E_{pol}	E_{dis}	E_{rep}	E_{tot}
x, y, z	5.35	−13.3	−2.6	−56.0	29.3	−46.7
$x + ½, −y + ½, −z$	6.44	−13.9	−2.0	−55.5	35.2	−42.7
$−x, y + ½, −z + ½$	9.99	−8.1	−2.2	−24.6	19.3	−19.8
$−x + ½, −y, z + ½$	11.63	−4.1	−1.0	−23.2	10.0	−19.1
$x + ½, −y + ½, −z$	14.41	12.9	−2.7	−30.1	0.0	−14.6
$−x, y + ½, −z + ½$	10.07	−2.8	−0.7	−19.5	12.3	−12.8
$−x + ½, −y, z + ½$	12.74	0.5	−0.3	−9.3	0.0	−7.7

In general, it is dispersion interactions that are dominant within the crystal structure, which is in line with the mentioned absence of hydrogen bonds. The basic structural unit of the crystal packing is revealed to be the herring-bone type arrangement of **L** molecules, forming a double-layered column lying parallel to the (0 2 −1) crystallographic plane, and infinitely propagating along the crystallographic *a* axis, as depicted in Fig 2a.
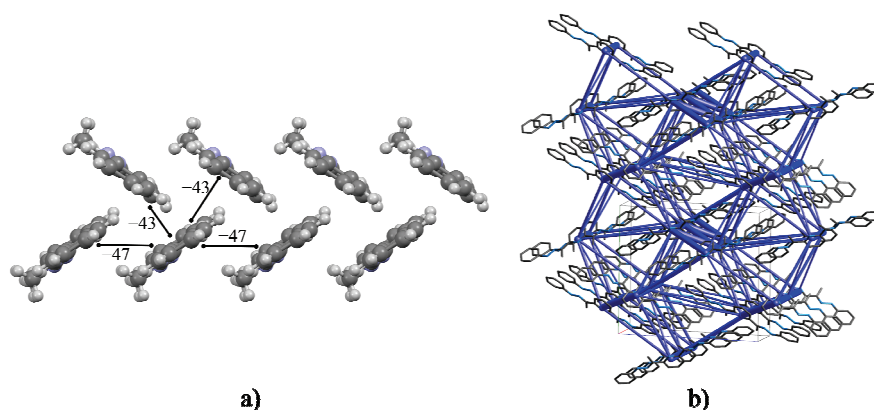

Fig. 2. a) Side view of the herring-bone type arrangement of **L** molecules; numbers indicate interaction energy in kJ mol^{-1}. b) Energy framework of the crystal structure of **L**.

From the perspective of an **L** molecule, the motif is realized by two different interactions, each forming two pairs. These interactions are dispersion dominated, but it is noteworthy that they are the only ones that make any significant electrostatic contribution to the stabilizing energy.

A stabilizing interaction of the energy of -47 kJ mol^{-1} is formed between two partner molecules, related by pure translations along crystallographic *a* axis. The molecules mutually form a stacking arrangement with significant offset. An energetically comparable (-43 kJ mol^{-1}) interaction is formed between the selected molecule of **L** from one sub-layer and two molecules belonging to the second sub-layer of the double layer motif. These molecules and **L** from the first sub-layer are related by 2_1 screw rotation along the crystallographic *b* axis, coupled to additional translations. Overview of crystal packing energetics is presented on an energy framework diagram (Fig. 2b), constructed from the calculated intermolecular energies.

Crystal structure of [Cu^{II}L$_2$][Cu$^I_2$Br$_4$] (1)

The crystal structure of complex **1** is comprised of isolated complex cations [CuL$_2$]$^{2+}$ and dinuclear complex anions [Cu$_2$Br$_4$]$^{2-}$. The molecular structure of the formula unit is shown in Fig. 3. The structure of the complex cation [CuL$_2$]$^{2+}$ was already described in a structurally characterized compound, [CuL$_2$]Br$_2$.[16] While the complex cation in [CuL$_2$]Br$_2$ has crystallographic two-fold symmetry, in **1** this symmetry is only approximate (two-fold pseudosymmetry axis bisects N2A–Cu1–N4B angle). Allowing for a large tolerance margin, the cation has D_2 point group symmetry, with additional two-fold axes passing through the N1A––Cu1–N1B bonds and cutting across the N2A–Cu1–N2B angle, respectively.
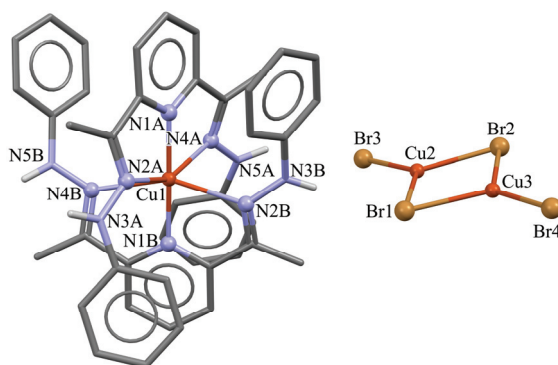

Fig. 3. Molecular structure of the formula unit of [Cu^{II}L$_2$][Cu$^I_2$Br$_4$] (**1**).

The ligand is coordinated as a tridentate, through the pyridine nitrogen atom and two imine nitrogen atoms, analogous to the mode found in [CoL$_2$]I$_2$ (CSD refcode ZIXSOR),[15] and resembling that of a structurally related ligand 2,6-di-

formylpyridine bis(phenylhydrazone), **L′**, in [Zn(**L′**)$_2$](CF$_3$O$_3$S)$_2$ (CSD refcode GUKTOW).[34] Two ligands are meridionally arranged in a very distorted octahedral environment of a Cu(II) ion, so that the dihedral angle is enclosed by mean planes through the Cu1, N1A, N2A and N4A atoms, and Cu1, N1B, N2B and N4B atoms, amounts 72.94(8)°, reflecting the deformation of the coordination polyhedron by its deviation from 90°. A deviation from the ideal octahedron is also manifested through *trans*-valence angles deviating from their ideal values of 180°, as shown in Table II.

TABLE II. Selected structural parameters of [Cu^{II}L$_2$][Cu$^{I}_2$Br$_4$] (**1**), [CuL$_2$]Br$_2$ and **L**

Bond	Bond length, Å	
	[Cu^{II}L$_2$][Cu$^{I}_2$Br$_4$] (**1**)	[CuL$_2$]Br$_2$[16]
Cu1–N1A	1.936(3)	1.9451(18)
Cu1–N1B	1.944(3)	–
Cu1–N2A	2.258(3)	2.2170(18)
Cu1–N2B	2.288(3)	–
Cu1–N4A	2.308(3)	2.3736(18)
Cu1–N4B	2.334(4)	
	Valence angle, °	
N1A–Cu1–N1B	176.75(14)	
N2A–Cu1–N4A	152.59(13)	
N2B–Cu1–N4B	152.58(13)	

	Bond length, Å		
	[Cu^{II}L$_2$][Cu$^{I}_2$Br$_4$] (**1**)		**L**
	Ligand A	Ligand B	
N1–C1	1.352(5)	1.358(5)	1.348(3)
N1–C5	1.347(5)	1.348(5)	1.339(3)
C1–C6	1.475(6)	1.461(6)	1.478(3)
C5–C8	1.464(6)	1.461(6)	1.483(3)
C6–N2	1.297(5)	1.294(6)	1.290(3)
C8–N4	1.300(5)	1.305(6)	1.287(3)
N2–N3	1.357(5)	1.349(5)	1.357(3)
N4–N5	1.353(5)	1.357(5)	1.358(3)

Metal–ligand bond lengths belonging to two ligand molecules, designated A and B in the atom enumeration scheme, are not equivalent. The shortest coordination bonds involve pyridine nitrogen atoms N1A and N1B, which have a comparable length with the one found in [CuL$_2$]Br$_2$. Mid-length bonds are longer in **1** than in [CuL$_2$]Br$_2$, while the longest bonds in **1** are shorter than the corresponding ones in [CuL$_2$]Br$_2$, thus manifesting the flexibility of the [CuL$_2$]$^{2+}$ cation. Intraligand bond lengths do not show significant differences between coordinated and free **L**, as shown in Table II.

In [Cu$_2$Br$_4$]$^{2-}$, the bromide ions are arranged in a trigonal-planar geometry around each copper(I) atom. By virtue of edge sharing, a four-membered metal-

locycle is formed, with two bromide ions in a bridging mode, and a Cu⋯Cu separation of 2.9477(8) Å. The four-membered ring Cu2–Br1–Cu3–Br2 can be regarded as flat for all practical purposes.

*Thermal properties of **L**, [Cu**L**$_2$]Br$_2$ and [Cu^{II}**L**$_2$][Cu^{I}$_2$Br$_4$] (**1**)*

The ligand, and both complexes were analyzed by simultaneous TG-DSC measurements. In an inert atmosphere, the ligand was stable up to relatively high temperature (Fig. 4). It melted at 220 °C and began to decompose at 250 °C, onset. Above this temperature, **L** loses about 80 % of its mass in one step up to 600 °C with a DTG maximum at 322 °C. The heat effect of thermal decomposition is exothermic with a peak maximum at 322 °C.
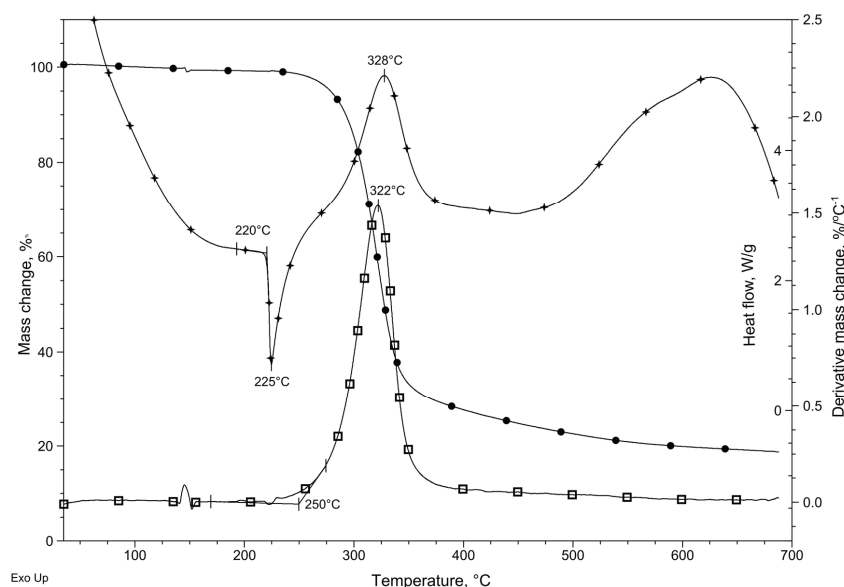
Fig. 4. TG (•), DTG (□) and DSC (+) curves of **L** in nitrogen.

The thermal stability of complexes is lower than that of the ligand and decreases in order: **L** (250 °C) > [Cu**L**$_2$]Br$_2$ (221 °C) > [Cu^{II}**L**$_2$][Cu^{I}$_2$Br$_4$] (212 °C). The mass loss in **1** began at 83 °C, onset and the mass decrease is 3.4 % (Fig. 5). The rate maximum of this process is achieved at 150 °C. By coupled TG–MS measurements, it was determined that this mass loss corresponds to evaporation of absorbed water (Fig. S-2 of the Supplementary material). The thermal decomposition of the complex started at 212 °C, onset, before the solvent loss was finished. This compound loses about 20 % of its mass up to 300 °C in a well-defined step with DTG maximum at 228 °C. Above this temperature, the decomposition was continuous, and its steps could not be distinguished. Only a small intensity DTG peak could be observed at 408 °C.
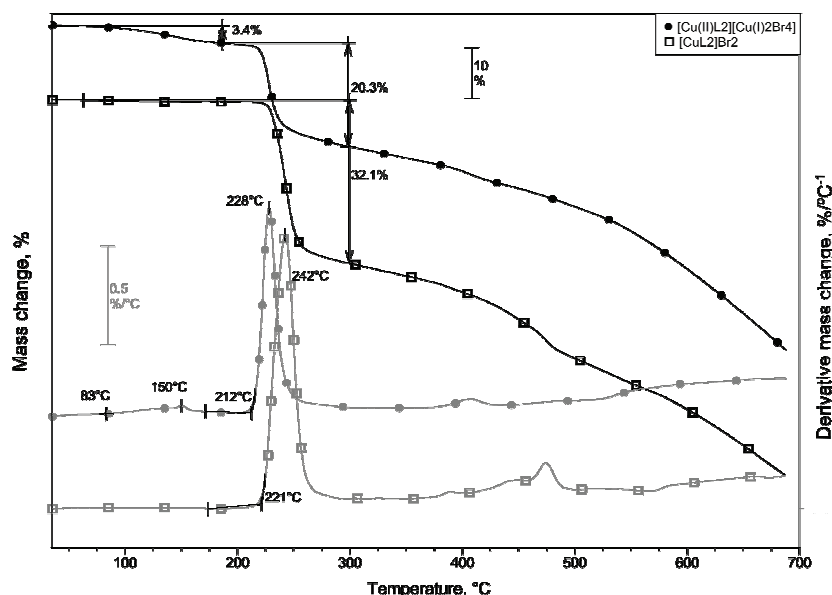
Fig. 5. TG and DTG curves of $[Cu^{II}L_2][Cu^I_2Br_4]$ (•) and $[CuL_2]Br_2$ (□) in nitrogen.

The thermal stability of $[CuL_2]Br_2$ is higher than that of $[Cu^{II}L_2][Cu^I_2Br_4]$, but also lower than the stability of the ligand. The sample of this compound did not contain any solvent and began to decompose at 221 °C, onset. Similarly to **1**, only one decomposition step was observed with a mass loss of 32.1 % and a DTG maximum at 242 °C. At higher temperatures, the decomposition processes are completely overlapped with a low intensity DTG peak at 475 °C.

The high thermal stability of the ligand and lower stabilities of the complexes show that coordination decreases the stability of the ligand. As the cation is the same in both complexes, their different thermal stabilities (comparing **1** after water loss) can be attributed to their counterions.

Complex **1** has the bulky tetracyclic $[Cu_2Br_4]^{2-}$ anion, as opposed to $[CuL_2]Br_2$, which possesses only two bromide ions, resulting in a significantly smaller counterion volume. Due to the voluminous complex anion, the packing of **1** is less compact than that of $[CuL_2]Br_2$. Therefore, the empty space in the crystal lattice of **1** is larger and water molecules are capable of occupying it.

The heat flow curves of the compounds (Fig. S-3 of the Supplementary material) show the same tendency. Namely, the solvent loss of **1** was endothermic. After that, the beginning of its thermal decomposition was also endothermic with a small peak at 220 °C, which almost immediately turned exothermic (233 °C). Above 300 °C, the decomposition was followed by an exothermic heat effect. Only slight differences were observed on the heat flow curve of $[CuL_2]Br_2$. Its decomposition also started with a small endothermic peak at 231 °C, followed by an

intensive exothermic one at 250 °C. The thermal decomposition processes above 300 °C were mostly exothermic (peak maxima at 441 and 479 °C) with a small endothermic peak at 471 °C.

CONCLUSIONS

The molecular structure of **L** revealed that the ligand adopts a conformation quite common to those of structurally related compounds. An assessment of the energetics of the intermolecular interactions in the crystal structure by computational methods revealed that dispersion interactions are dominant. The basic structural unit of the crystal packing is the herring-bone type arrangement of **L** molecules.

The composition of the obtained complexes depended not only on the $CuBr_2$ to **L** mole ratio, but also on the nature of the reaction solvent involved. In the complex cation of **1**, the ligand is coordinated as a tridentate N_3, and two ligand molecules are meridionally arranged in a very distorted octahedral environment around the Cu(II) ion. In $[Cu_2Br_4]^{2-}$, bromides are arranged in a trigonal-planar geometry around each copper(I) atom; with two bromides in a bridging mode, forming a four-membered metallocycle.

The relatively high thermal stability of the ligand decreases on coordination to the Cu^{II} ion. As the cation is identical in both complexes, the difference in their thermal stability could be ascribed to the anions present. Due to the bulky $[Cu_2Br_4]^{2-}$ anion, the packing of **1** is less compact than that of $[CuL_2]Br_2$.

SUPPLEMENTARY MATERIAL

Additional data and information are available electronically at the pages of journal website: https://www.shd-pub.org.rs/index.php/JSCS/article/view/11422, or from the corresponding author on request.

И З В О Д
РЕАКЦИЈЕ БАКАР(II)-БРОМИДА СА БИС(ФЕНИЛХИДРАЗОНОМ)
2,6-ДИАЦЕТИЛПИРИДИНА (**L**) – МОЛЕКУЛСКА И КРИСТАЛНА СТРУКТУРА
L И ЊЕГОВОГ МЕШОВИТО-ВАЛЕНТНОГ КОМПЛЕКСА [Cu^II L_2][Cu^I_2Br_4]

МАРКО В. РОДИЋ[1], МИРЈАНА М. РАДАНОВИЋ[1], ДРАГАНА В. ГАЗДИЋ[1], ВУКАДИН М. ЛЕОВАЦ[1], БЕРТА БАРТА ХОЛО[1], ВИДАК РАИЧЕВИЋ[1], СВЕТЛАНА К. БЕЛОШЕВИЋ[2], БИЉАНА КРИГЕР[3] и ЛИЉАНА С. ВОЈИНОВИЋ-ЈЕШИЋ[1]

[1]*Универзитет у Новом Саду, Природно–математички факултет, Трг Д. Обрадовића 3, 21000 Нови Сад,* [2]*Факултет техничких наука, Универзитет у Приштини, Књаза Милоша 7, 38220 Косовска Митровица и* [3]*University of Innsbruck, Institute of Mineralogy and Petrography, Innrain 52, 6020 Innsbruck, Austria*

Кристална и молекулска структура бис(фенилхидразона) 2,6-диацетилпиридина, **L**, одређене су рендгенском структурном анализом. Енергије интермолекулских интеракција

у кристалној структури су процењене рачунарским методама и имају доминантно дисперзиони карактер. Основна структурна јединица кристалног паковања настаје слагањем молекула **L** у мотив облика рибље кости. Асигнација IR спектра **L** је извршена помоћу DFT прорачуна. У раду су описане нове реакције **L** са $CuBr_2$ у којима настаје валентно-мешовити Cu(II)–Cu(I) комплекс формуле $[Cu^{II}L_2][Cu^{I}_2Br_4]$ (**1**), који је структурно окарактерисан. У комплексном катјону су два молекула лиганда меридијално распоређена око Cu(II), градећи веома деформисано октаедарско окружење. У анјону су бромидни јони распоређени тригонално-планарно око јона Cu(I). Описана су термичка својства лиганда, комплекса **1** и претходно синтетисаног комплекса $[CuL_2]Br_2$. Термичка стабилност комплекса је нижа од термичке стабилности лиганда: **L** (250 °C) > $[CuL_2]Br_2$ (221 °C) > > $[Cu^{II}L_2][Cu^{I}_2Br_4]$ (212 °C). Разлика у термичкој стабилности комплекса може да се припише различитој ефикасности паковања јона у кристалним структурама.

REFERENCES

1. D. G. Guimarães, L. A. Rolim, A. de A. Gonsalves, C. R. M. Araújo, *Rev. Virtual Química* **9** (2017) 2551 (https://dx.doi.org/10.21577/1984-6835.20170151)
2. C. Bonaccorso, T. Marzo, D. La Mendola, *Pharmaceuticals* **13** (2020) (https://dx.doi.org/10.3390/ph13010004)
3. S. Rollas, S. Küçükgüzel, S. Rollas, S. G. Küçükgüzel, *Molecules* **12** (2007) 1910 (https://dx.doi.org/10.3390/12081910)
4. M. M. E. Shakdofa, M. H. Shtaiwi, N. Morsy, T. M. A. Abdel-rassel, *Main Gr. Chem.* **13** (2014) 187 (https://dx.doi.org/10.3233/MGC-140133)
5. A.-M. Stadler, J. Harrowfield, *Inorg. Chim. Acta* **362** (2009) 4298 (https://dx.doi.org/10.1016/j.ica.2009.05.062)
6. M. Katyal, Y. Dutt, *Talanta* **22** (1975) 151 (https://dx.doi.org/10.1016/0039-9140(75)80161-5)
7. Y. P. Kitaev, *Khimiya gidrazonov*, Nauka, Moscow, 1977
8. Y. P. Kitaev, B. I. Buzykin, *Gidrazony*, Nauka, Moscow, 1974
9. I. D. Kostas, B. R. Steele, *Catalysts* **10** (2020) art. no. 1107 (https://dx.doi.org/10.3390/catal10101107)
10. V. V. Kogan, V.A., Zelentsov, V.V., Larin, G. M., Lukov, *Kompleksy perekhodnykh metallov s gidrazonami*, Nauka, Moscow, 1990
11. J. D. Curry, M. A. Robinson, D. H. Busch, *Inorg. Chem.* **6** (1967) 1570 (https://dx.doi.org/10.1021/ic50054a032)
12. I. Ivanović-Burmazović, K. Anđelković, in *Advances in Inorganic Chemistry*, R. van Eldik, Ed., Academic Press, Cambridge, MA, 2004, p. 315 (https://dx.doi.org/10.1016/S0898-8838(03)55006-1)
13. C. A. Brown, W. Kaminsky, K. A. Claborn, K. I. Goldberg, D. X. West, *J. Braz. Chem. Soc.* **13** (2002) 10 (https://dx.doi.org/10.1590/S0103-50532002000100003)
14. T. S. Lobana, R. Sharma, G. Bawa, S. Khanna, *Coord. Chem. Rev.* **253** (2009) 977 (https://dx.doi.org/10.1016/J.CCR.2008.07.004)
15. S. Belošević, M. Rodić, M. Radanović, V. Leovac, *Univ. Thought - Publ. Nat. Sci.* **8** (2018) 33 (https://dx.doi.org/10.5937/UNIVTHO8-19451)
16. S. Belošević, M. M. Radanović, M. V. Rodić, V. M. Leovac, *Bull. Nat. Sci. Res.* **11** (2021) 24 (https://dx.doi.org/10.5937/BNSR11-30567)
17. Rigaku Oxford Diffraction, *CrysAlisPro Software system*, Rigaku Corporation, Wroclaw, 2021

18. G. M. Sheldrick, *Acta Crystallogr., A* **71** (2015) 3 (https://dx.doi.org/10.1107/S2053273314026370)
19. G. M. Sheldrick, *Acta Crystallogr., C* **71** (2015) 3 (https://dx.doi.org/10.1107/S2053229614024218)
20. C. B. Hübschle, G. M. Sheldrick, B. Dittrich, *J. Appl. Crystallogr.* **44** (2011) 1281 (https://dx.doi.org/10.1107/S0021889811043202)
21. P. R. Spackman, M. J. Turner, J. J. McKinnon, S. K. Wolff, D. J. Grimwood, D. Jayatilaka, M. A. Spackman, *J. Appl. Crystallogr.* **54** (2021) 1006 (https://dx.doi.org/10.1107/S1600576721002910)
22. C. F. Mackenzie, P. R. Spackman, D. Jayatilaka, M. A. Spackman, *IUCrJ* **4** (2017) 575 (https://dx.doi.org/10.1107/S205225251700848X)
23. D. Jayatilaka, D. J. Grimwood, in *Proceeding of International Conference on Computational Science*, 2003, Melbourne, Australia and St. Petersburg, Russia, 2003 Proceedings, Part IV, Springer, 2003, p. 142 (https://dx.doi.org/10.1007/3-540-44864-0_15)
24. G. M. J. Barca, C. Bertoni, L. Carrington, D. Datta, N. De Silva, J. E. Deustua, D. G. Fedorov, J. R. Gour, A. O. Gunina, E. Guidez, T. Harville, S. Irle, J. Ivanic, K. Kowalski, S. S. Leang, H. Li, W. Li, J.J. Lutz, I. Magoulas, J. Mato, V. Mironov, H. Nakata, B.Q. Pham, P. Piecuch, D. Poole, S.R. Pruitt, A.P. Rendell, L.B. Roskop, K. Ruedenberg, T. Sattasathuchana, M.W. Schmidt, J. Shen, L. Slipchenko, M. Sosonkina, V. Sundriyal, A. Tiwari, J.L. Galvez Vallejo, B. Westheimer, M. Włoch, P. Xu, F. Zahariev, M.S. Gordon, *J. Chem. Phys.* **152** (2020) 154102 (https://dx.doi.org/10.1063/5.0005188)
25. B. M. Bode, M. S. Gordon, *J. Mol. Graph. Model.* **16** (1998) 133 (https://dx.doi.org/10.1016/s1093-3263(99)00002-9)
26. W. J. Geary, *Coord. Chem. Rev.* **7** (1971) 81 (https://dx.doi.org/10.1016/S0010-8545(00)80009-0)
27. L. S. Vojinović-Ješić, M. M. Radanović, *Coordination chemistry of aminoguanidine and its Schiff bases*, Faculty of Sciences, Novi Sad, 2017 (in Serbian)
28. H. Günzler, H.-U. Gremlich, *IR-Spektroskopie: Eine Einführung, Fourth Edition*, John Wiley & Sons, Ltd., Weinheim, 2003, pp. 157–264 (https://dx.doi.org/10.1002/9783527662852.ch6)
29. K. Nakamoto, *Infrared and Raman Spectra of Inorganic and Coordination Compounds*, John Wiley & Sons, Inc., Hoboken, NJ, 2008
30. C. R. Groom, I. J. Bruno, M. P. Lightfoot, S. C. Ward, *Acta Crystallogr., B* **72** (2016) 171 (https://dx.doi.org/10.1107/S2052520616003954)
31. W. Clegg, R. W. Harrington, *CSD Commun.*, Database Identifier KEWWOB, Deposition Number 1836923 (2018) (https://dx.doi.org/10.5517/ccdc.csd.cc1znglp)
32. W. Radecka-Paryzek, M. Kubicki, E. Luks, *Struct. Chem.* **21** (2010) 299 (https://dx.doi.org/10.1007/s11224-009-9532-y)
33. C. Jelsch, K. Ejsmont, L. Huder, *IUCrJ* **1** (2014) 119 (https://dx.doi.org/10.1107/S2052252514003327)
34. F. Dumitru, Y.-M. Legrand, M. Barboiu, E. Petit, A. van der Lee, *Cryst. Growth Des.* **9** (2009) 2917 (https://dx.doi.org/10.1021/cg9002466).